ION CYCLOTRON EMISSION FROM FUSION PRODUCTS AND BEAM IONS IN THE TOKAMAK FUSION TEST REACTOR

T. FÜLÖP, M. LISAK
Department of Electromagnetics,
Chalmers University of Technology and Euratom–NFR Association,
Göteborg, Sweden

ABSTRACT. Ion cyclotron emission (ICE) observed during deuterium and deuterium–tritium experiments in TFTR can be driven by both fusion products and injected beam ions. The emission driven by fusion products is a result of the excitation of the fast magnetoacoustic wave through toroidicity affected cyclotron resonance, the magnetoacoustic cyclotron instability. For beam driven ICE, the excitation mechanism, outlined by R.O. Dendy et al. (Phys. Plasmas **1** (1994) 3407) for the cylindrical case, is generalized by including the curvature and ∇B drift in the local resonance condition. The phase velocity of the destabilized, predominantly electrostatic, wave is typically an order of magnitude smaller than the Alfvén velocity. For both fusion and beam driven ICE, it is found that the instability growth rate is greatly increased as compared with the cylindrical case and reaches its maximum for nearly perpendicular propagation. The results of the numerical and analytical stability analysis are consistent with the experimental observations and provide an explanation for the simultaneous excitation of sequential multiple cyclotron harmonics of the fast ions, the sublinear correlation of the growth rate with the fast ion density and the stabilizing effect of the increasing fast ion velocity spread.

1. INTRODUCTION

Ion cyclotron emission (ICE) has been observed during deuterium and deuterium–tritium experiments in TFTR [1, 2]. A theoretical understanding of the ICE excitation and propagation mechanism may allow us to extract information about the properties of the energetic ion population. Ion cyclotron emission, as an additional diagnostic tool, could thereby contribute to the successful operation of fusion reactors.

Similar ICE has been observed in several other tokamak experiments [3–6]. In all cases the emission is driven by a population of energetic ions, and in all the major tokamaks the ICE source is localized to the outer midplane. However, some of the features of the observed spectral lines are different, for example, the ICE observed in JET is driven only by fusion products (not the injected beam ions) and persists during the whole discharge [4], whereas at the beginning (the first 100 to 250 ms) of the TFTR discharge the emission spectrum consists of intense narrow peaks at multiple harmonics of the cyclotron frequency of the fusion products. Later, these peaks are replaced (over the next 100 ms) by those of the injected beam ions [2, 7–9]. For both the initial and final spectra, the emission source is localized to the outer midplane region, where both the fusion products and the beam ions have an anisotropic velocity distribution. Another difference is that the ICE intensity in JET is proportional to the neutron rate, while the correlation in TFTR is sublinear and scattered. The differences between the typical JET and TFTR ICE observations are attributed to the sensitivity of the instability growth rate to the ratio between the velocity of the alpha particles and the local Alfvén velocity. In the JET outer midplane region, the fusion produced alpha particles are super-Alfvénic, while in TFTR the birth velocity of the alpha particles is about one half of the local Alfvén velocity, cf. Ref. [10].

The emission observed in JET has been thoroughly investigated [11, 12] and is attributed to the magnetoacoustic cyclotron instability (MCI). The MCI is based on the resonant wave–particle interaction between the fast magnetoacoustic wave and the energetic ions. The theory of the MCI, originally restricted to the straight magnetic field approximation, was recently generalized to the toroidal case in Ref. [12] by including the curvature and ∇B drift (called in the following 'toroidal drift') in the resonance condition. This new toroidicity affected resonance has been shown to be of importance, as it provides an explanation of the main features of the ICE spectrum observed at JET.

Recent theoretical investigations of the TFTR data [8, 13], using the straight magnetic field approximation, have suggested that the same mechanism (MCI) is responsible for the excitation of the fusion

driven ICE. It has been shown that the MCI is suppressed if the sub-Alfvénic fusion products slow down, which is in agreement with the observations. In Ref. [13] the time evolution of the ICE has also been investigated. The predicted time evolution agrees qualitatively with that observed for the 'early' (fusion product driven) emission, i.e. the ICE should be observed during the first 100 ms of the beam injection, and the peak intensity should reach its maximum after about 40 ms. However, for the rapid instability, considered in Ref. [13], the instability growth rate γ should be larger than the fast ion inverse bounce period τ_b, a condition that is not fulfilled, for the results of Ref. [13], unless the fast particle density is much higher than the estimated values near the Alfvén edge.

The beam driven ICE has been theoretically investigated in Ref. [9]. As the fast ion velocities are far below the Alfvén velocity, it is sufficient to consider the electrostatic limit of the dispersion relation. The destabilized waves have phase velocities ω/k about an order of magnitude smaller than the Alfvén velocity.

In the present article we present numerical results which show that the inclusion of the toroidal effects in the resonance condition increases the growth rate of the MCI and yields growth rates that satisfy the rapid instability condition, $\gamma > \tau_\mathrm{b}^{-1}$. The article explains some of the main features of the ICE spectrum observed at TFTR, such as the strong growth rates for perpendicularly propagating waves, which yield spectral peaks localized at sequential cyclotron harmonics of the energetic ions, the growth rate scaling with the neutron rate and the stabilizing effect of the increasing fast ion velocity spread.

Following the approach of Ref. [12], we consider local theory and rapid instability, $\gamma > \tau_\mathrm{b}^{-1}$, and include the effect of the fast ion toroidal drift frequency in the resonance condition. The instability growth rates are calculated numerically by solving the full dispersion equation and then the results are used to investigate the dependence of the growth rate on propagation angle, fast ion density and fast ion parallel velocity spread.

The article is structured as follows: in Section 2, we describe briefly the theoretical background of the magnetoacoustic cyclotron instability and derive simple perturbative expressions for the growth rate of both fusion and beam ion driven instabilities. In Section 3, we present the results of a numerical study of the dispersion equation for both fusion product and beam ion driven instabilities. The instability growth rates are calculated and compared with the analytical predictions of Section 2. Finally, Section 4 is devoted to conclusions.

2. STABILITY OF FAST MAGNETOACOUSTIC WAVES

Following the approach of Ref. [12], we have investigated the solutions of the dispersion relation for the fast magnetoacoustic waves,

$$\left(\epsilon_{11} - \frac{k_\parallel^2 c^2}{\omega^2}\right)\left(\epsilon_{22} - \frac{k^2 c^2}{\omega^2}\right) + \epsilon_{12}^2 = 0 \tag{1}$$

where ϵ_{ij} are the dielectric tensor elements, ω is the wave frequency, k is the wavenumber, $k_\parallel$ is the component of the wavevector parallel to the magnetic field and c is the speed of light. In the derivation of Eq. (1) we have used the local approximation and assumed that the wave electric field was approximately polarized in the plane perpendicular to the magnetic field direction.

The dielectric tensor components contain contributions from electrons, bulk ions and energetic ions (denoted by the superscripts e, i and α, respectively): $\epsilon_{ij} = \delta_{ij} + \epsilon_{ij}^\mathrm{e} + \epsilon_{ij}^\mathrm{i} + \epsilon_{ij}^\alpha$, where δ_{ij} is the Kronecker delta. The corresponding expressions for electrons and bulk ions having Maxwellian velocity distributions, taken in the limit $\omega \ll \omega_\mathrm{ce}$ and $a_\mathrm{e} \equiv k_\perp^2 v_\mathrm{e}^2/2\omega_\mathrm{ce}^2 \ll 1$, where v_e is the electron thermal velocity and $k_\perp$ is the component of the wavevector perpendicular to the magnetic field, are given in Ref. [11]. For the electrons we have

$$\epsilon_{11}^\mathrm{e} = \frac{\omega_\mathrm{pe}^2}{\omega_\mathrm{ce}^2}, \quad \epsilon_{12}^\mathrm{e} = \mathrm{i}\frac{\omega_\mathrm{pe}^2}{\omega\omega_\mathrm{ce}} \tag{2a,b}$$

and

$$\epsilon_{22}^\mathrm{e} = 2\frac{\omega_\mathrm{pe}^2}{\omega^2} a_\mathrm{e}\zeta_\mathrm{e} Z(\zeta_\mathrm{e}) \tag{2c}$$

where the frequencies ω_pe and ω_ce are the plasma and cyclotron frequencies of the electrons, respectively, and Z is the plasma dispersion function with the argument $\zeta_\mathrm{e} = \omega/k_\parallel v_\mathrm{e}$. The corresponding expressions for the bulk ions are

$$\epsilon_{11}^\mathrm{i} = \frac{\omega_\mathrm{pi}^2}{\omega^2} \sum_{l=-\infty}^{\infty} \frac{l^2 \mathrm{e}^{-a_\mathrm{i}} I_l}{a_\mathrm{i}} \zeta_0 Z(\zeta_l) \tag{3}$$

$$\epsilon_{22}^\mathrm{i} = \frac{\omega_\mathrm{pi}^2}{\omega^2} \sum_{l=-\infty}^{\infty} \left(\frac{l^2 \mathrm{e}^{-a_\mathrm{i}} I_l}{a_\mathrm{i}} + 2a_\mathrm{i}\mathrm{e}^{-a_\mathrm{i}}(I_l - I_l') \right) \zeta_0 Z(\zeta_l) \tag{4}$$

$$\epsilon_{12}^{\mathrm{i}} = \mathrm{i}\frac{\omega_{\mathrm{pi}}^2}{\omega^2}\sum_{l=-\infty}^{\infty} l\mathrm{e}^{-a_{\mathrm{i}}}(I_l - I_l')\zeta_0 Z(\zeta_l) \quad (5)$$

where the argument of the plasma dispersion function is $\zeta_l = (\omega - l\omega_{\mathrm{ci}})/(k_\parallel v_{\mathrm{i}})$, $I_l = I_l(a_{\mathrm{i}})$ is the modified Bessel function of the first kind of order l with the argument $a_{\mathrm{i}} = k_\perp^2 v_{\mathrm{i}}^2/2\omega_{\mathrm{ci}}^2$, $I_l' = \partial I_l/\partial a_{\mathrm{i}}$, ω_{pi} and ω_{ci} are the plasma and cyclotron frequencies, respectively, and v_{i} is the thermal velocity of the bulk ions. The expressions for the dielectric tensor components for energetic ions are determined by, cf. Ref. [12],

$$\epsilon_{ij}^{\alpha} = \sum_{s=-\infty}^{\infty}\frac{\omega_{\mathrm{p}\alpha}^2}{\omega^2}\int \mathrm{d}^3 v \frac{v_\perp^2\hat{\Pi}f_\alpha}{\omega - k_\parallel v_\parallel - s\omega_{\mathrm{c}\alpha} - \omega_{\mathrm{D}}}M_{ij}(s,\xi) \quad (6)$$

where

$$M_{ij}(s,\xi) = \begin{pmatrix} (s^2/\xi^2)J_s^2(\xi) & -(\mathrm{i}s/\xi)J_s(\xi)J_s'(\xi) \\ (\mathrm{i}s/\xi)J_s(\xi)J_s'(\xi) & [J_s'(\xi)]^2 \end{pmatrix} \quad (7)$$

$$\hat{\Pi} = \omega\frac{\partial}{\partial E} + \frac{\omega - k_\parallel v_\parallel - \omega_{\mathrm{D}}}{B_0}\frac{\partial}{\partial \mu}. \quad (8)$$

Here, B_0 is the equilibrium magnetic field strength, μ is the fast ion magnetic moment and E is the fast ion energy (both per unit mass), $J_s(\xi)$ is the Bessel function of the first kind and of order s, $J_s'(\xi) = \partial J_s/\partial\xi$, f_α is the unperturbed velocity distribution function of the fast ions, $\xi = k_\perp v_\perp/\omega_{\mathrm{c}\alpha}$, $\omega_{\mathrm{c}\alpha}$ is the fast ion cyclotron frequency, $\omega_{\mathrm{D}} = -mv_{\mathrm{D}}/r$, $v_{\mathrm{D}} = v^2(1+\chi^2)/(2\omega_{\mathrm{c}\alpha}R)$ is the toroidal drift velocity where m is the poloidal wavenumber and $\chi = v_\parallel/v$ is the pitch angle variable. Note that the guiding centre drift in the toroidal direction is $O(\epsilon)$ as compared with the poloidal drift component and therefore it can be neglected.

The instability growth rate is calculated by solving Eq. (1) numerically, for the experimental parameters at the outer midplane edge. Following the spirit of Refs [9, 11], we model the velocity distribution function of the energetic ions with a drifting ring with a Maxwellian spread of velocities parallel to the magnetic field

$$f_\alpha = \frac{1}{2\pi^{3/2}uv_{\mathrm{s}}}\exp\left(-\frac{(v_\parallel - v_{\mathrm{d}})^2}{v_{\mathrm{s}}^2}\right)\delta(v_\perp - u) \quad (9)$$

where u is the perpendicular velocity of the fast ions, and v_{d} and v_{s} denote the parallel velocity drift and the velocity spread, respectively. Note that v_{d} is different from the toroidal drift velocity, denoted by v_{D}. The fusion ion distribution at the outer midplane plasma edge is well approximated by this distribution function [2, 11], since the fusion ion population in that region is dominated by centrally born ions having barely trapped orbits that carry them to the outer midplane edge. Note that only those centrally born fusion ions that have energies above a certain threshold undergo radial excursions to the outer midplane edge [13]. This gives rise to a population inversion at the outer midplane, even when the fusion products in the plasma centre have a slowed down distribution. The use of the same distribution function to describe beam ions is also reasonable because these ions can be assumed to have a narrow distribution of velocities parallel to the magnetic field, close to the point of beam injection in the edge plasma. The numerical values of the parameters v_{d}, v_{s} and u are different for beam and fusion ions. This distribution function allows us to perform the integrations in Eq. (6) analytically (expressed in terms of the plasma dispersion function), thus saving a considerable amount of computer time (see Appendix for details).

2.1. Perturbative analysis

We consider waves with exponentially small damping due to thermal plasma particles by assuming that $|\zeta_{\mathrm{e}}| \gg 1$ and $|\zeta_l| \gg 1$. This assumption is justified for nearly perpendicularly propagating waves. Assuming also that $1 \ll (\omega/\omega_{\mathrm{ci}})^2 \ll M_{\mathrm{i}}/M_{\mathrm{e}}$ (M denotes the particle mass), as well as $k_\parallel^2 c^2/\omega_{\mathrm{pi}}^2 \ll 1$, the dispersion relation for the fast magnetoacoustic waves can be simplified to [12]

$$\omega_{\mathrm{pi}}^2\left(\frac{1}{\omega^2} - \frac{1}{k^2 v_{\mathrm{A}}^2}\right) = \epsilon_{11}^{\alpha}(\omega, k) \quad (10)$$

where v_{A} is the Alfvén velocity. Putting $\omega = \omega_0 + \delta\omega$, with $\omega_0 = kv_{\mathrm{A}} \simeq l\omega_{\mathrm{c}\alpha} + k_\parallel v_{\mathrm{d}} + \omega_{\mathrm{D}}$ and $|\delta\omega| \ll \omega_0$, we can expand Eq. (10) around ω_0 and obtain

$$-\omega_{\mathrm{pi}}^2\frac{2\delta\omega}{\omega_0^3} = \epsilon_{11}^{\alpha}(\omega_0, k) + \delta\omega\left(\frac{\partial\epsilon_{11}^{\alpha}}{\partial\omega}\right)_{\omega_0} \quad (11)$$

which with $\delta\omega = \delta\omega_{\mathrm{r}} + \mathrm{i}\gamma^{\alpha}$ leads to

$$\gamma^{\alpha} = -\frac{1}{1+C^2}\frac{\mathrm{Im}\,\epsilon_{11}^{\alpha} - C\mathrm{Re}\,\epsilon_{11}^{\alpha}}{\mathrm{Re}\left(\dfrac{\partial\epsilon_{11}^{\alpha}}{\partial\omega}\right)_{\omega_0} + \dfrac{2\omega_{\mathrm{pi}}^2}{\omega_0^3}} \quad (12)$$

where

$$C = \frac{\mathrm{Im}\left(\dfrac{\partial\epsilon_{11}^{\alpha}}{\partial\omega}\right)_{\omega_0}}{\mathrm{Re}\left(\dfrac{\partial\epsilon_{11}^{\alpha}}{\partial\omega}\right)_{\omega_0} + \dfrac{2\omega_{\mathrm{pi}}^2}{\omega_0^3}}. \quad (13)$$

Equation (12) allows us to investigate the correlation between the fast ion density and the growth rate. As ϵ_{11}^{α} is proportional to n_α, one obtains for very small values of n_α, when $\mathrm{Re}\,(\partial\epsilon_{11}^{\alpha}/\partial\omega)_{\omega_0} \ll 2\omega_{\mathrm{pi}}^2/\omega_0^3$ and C is small, that

$$\frac{\gamma^{\alpha}}{\omega_0} = \frac{-\omega_0^2\,\mathrm{Im}\,\epsilon_{11}^{\alpha}}{2\omega_{\mathrm{pi}}^2} \tag{14}$$

which predicts a linear correlation between the fast ion density and the growth rates. In the other limit, for higher fast ion densities, when $\mathrm{Re}\,(\partial\epsilon_{11}^{\alpha}/\partial\omega)_{\omega_0} \gg 2\omega_{\mathrm{pi}}^2/\omega_0^3$, the growth rate tends to be independent of the fast ion density. For intermediate values of n_α, the growth rate dependence on n_α/n_{i} becomes sublinear.

The difference between the JET and TFTR scalings of the growth rate on n_α seems to be caused by the difference in the local (edge) Alfvén velocities. In TFTR the local Alfvén velocity is higher than the alpha particle velocity. Since $\omega_{\mathrm{pi}}^2/\omega_{\mathrm{ci}}^2 = c^2/v_{\mathrm{A}}^2$, the high Alfvén velocity leads to $\mathrm{Re}\,(\partial\epsilon_{11}^{\alpha}/\partial\omega)_{\omega_0} \gg 2\omega_{\mathrm{pi}}^2/\omega_0^3$, giving a weak sublinear correlation with the fast ion density. If the local Alfvén velocity is comparatively low, as in the case of JET, $\mathrm{Re}\,(\partial\epsilon_{11}^{\alpha}/\partial\omega)_{\omega_0} \ll 2\omega_{\mathrm{pi}}^2/\omega_0^3$, and then we obtain the linear correlation as given by Eq. (14). The threshold value of n_α/n_{i}, for which $\mathrm{Re}\,(\partial\epsilon_{11}^{\alpha}/\partial\omega)_{\omega_0}$ starts to play a role, is 10^{-6} in TFTR, while in JET it is about an order of magnitude higher, owing to the fact that the quantity $\omega_{\mathrm{pi}}^2/\omega_0^3$ is 20 times larger for the JET experimental parameters than for TFTR.

2.2. Electrostatic limit

Since the beam ion velocities are far below the Alfvén velocity, the perturbative solution given by Eq. (12) is not valid for the beam driven ICE. In the derivation of Eq. (12) it was assumed that the phase velocity of the destabilized wave is close to the Alfvén velocity. However, in the beam driven case the phase velocity of the destabilized wave turns out to be close to the beam ion velocity, which is about an order of magnitude less than the Alfvén velocity ($\omega/k \simeq v_{\mathrm{beam}} \ll v_{\mathrm{A}}$). In this case, it is sufficient to consider the electrostatic limit of the dispersion equation, which for perpendicular propagation can be written as

$$f(\omega) = 1 + \epsilon_{11}^{\mathrm{i}} + \epsilon_{11}^{\mathrm{b}} = 0 \tag{15}$$

where $\epsilon_{11}^{\mathrm{b}}$ denotes the dielectric tensor contribution from the beam ions. For frequencies in the ion cyclotron range, the electron terms can be neglected in the above equation. The solution of Eq. (15) is obtained by setting $\omega = \omega_0 + \delta\omega_{\mathrm{r}} + \mathrm{i}\gamma$, where $\omega_0 \simeq l\omega_{\mathrm{cb}} + k_\parallel v_{\mathrm{d}} + \omega_{\mathrm{D}}$, $|\delta\omega_{\mathrm{r}} + \mathrm{i}\gamma| \ll \omega_0$ and then expanding $\epsilon_{11}(\omega, k)$ around ω_0. This gives a perturbative solution for the instability growth rate, similar to Eq. (12):

$$\gamma^{\mathrm{b}} = -\mathrm{Im}\frac{f(\omega_0)[f'(\omega_0)]^{\star}}{|f'(\omega_0)|^2} = -\frac{1}{1+C^2}\frac{\mathrm{Im}\,\epsilon_{11}(\omega_0) - C\mathrm{Re}\,\epsilon_{11}(\omega_0)}{\mathrm{Re}\,\epsilon'_{11}(\omega_0)} \tag{16}$$

where $C = (\mathrm{Im}\,\epsilon'_{11}/\mathrm{Re}\,\epsilon'_{11})_{\omega_0}$, the prime denotes the derivative with respect to ω and the asterisk denotes complex conjugation. Unfortunately, this simple perturbative solution of the dispersion relation does not agree well with the numerically obtained behaviour of the instability growth rate in the beam driven case; for beam densities $n_{\mathrm{b}} > 10^{-6}\,n_{\mathrm{i}}$. However, in the fusion product driven case, the perturbative solution follows rather closely the numerically computed one, and therefore Eq. (12) can be used for understanding and estimating the dependence of the instability growth rate driven by fusion products on the fast ion density.

3. ION CYCLOTRON EMISSION IN TFTR

We now proceed to the analysis of the experimental observations in typical TFTR deuterium–deuterium (DD) and deuterium–tritium (DT) experiments. At the onset of beam injection, spectral lines corresponding to the alpha particle and ^{3}He harmonics (the fusion products) appear within 50 ms, but after 100 to 250 ms they disappear and are replaced by new harmonics of deuterium and tritium (the injected species) [2, 7, 8]. The initial ICE spectrum shows peaks corresponding to the fusion product cyclotron frequencies and is assumed to be caused mainly by the fusion products that are born near the plasma core and then follow barely trapped orbits, reaching the edge plasma shortly after the onset of neutral beam injection. Since the beam ions are injected parallel to the magnetic axis, they cannot initially have trapped orbits. Note that only at the plasma edge is the beam ion distribution sufficiently narrow for the growth rate to be high enough. Consequently, the initial spectrum will be dominated by the fusion product driven ICE, but later, when the beam particles have reached the edge plasma, they will also contribute to the final ICE spectrum.

In this section, we investigate the fusion and beam driven ICE and calculate the instability growth rate of the fast magnetoacoustic waves by solving the full dispersion equation numerically for typical parameters of the DT experiments in TFTR.

3.1. Fusion product driven ICE

We assume that the magnetic field $B_0 = 5$ T, the major radius of the torus $R = 2.52$ m, the minor radius $a = 0.87$ m, the edge Alfvén velocity $v_A = 2.2 \times 10^7$ m/s, the bulk ion beta $\beta_i = 10^{-4}$ [10] and the ratio of the alpha particle density to the bulk ion density $n_\alpha(r_\star)/n_i(r_\star) = 10^{-4}$, where $r_\star$ is the mode localization radius [14]. This localization radius, $r_\star$, is close to the outer midplane edge. The birth energies of the fusion products are 1, 0.82, 3.08 and 3.52 MeV for tritons, ^{3}He nuclei, protons and alpha particles, respectively, and the corresponding velocities are $v_T = 0.36v_A$, $v_{He} = 0.33v_A$, $v_p = 1.1v_A$ and $v_\alpha = 0.6v_A$. We note that the tritons, ^{3}He nuclei and alpha particles are sub-Alfvénic, in contrast to the JET DT experiment, where all the fusion products are super-Alfvénic. To model the energetic particle distribution, a drifting ring distribution function is used, with the drift velocity $v_d = -0.5u$, and the velocity spread $v_s = 0.05u$ for all four fusion products, cf. Ref. [13], and with the perpendicular velocities as follows: $u/v_A = 0.3$ (T, ^{3}He), 1 (p) and 0.5 (^{4}He). The background plasma is assumed to be pure deuterium.

The numerical results show that the destabilization takes place at frequencies $\omega \simeq kv_A \simeq l\omega_c + k_\parallel v_\parallel \pm |\omega_D|$ and that the instability growth rate is maximal for nearly perpendicular wave propagation ($k_\parallel \simeq 0$). The values of the poloidal wavenumbers are approximately given by the integer part of $(l\omega_{c\alpha}/v_A)r_\star$, where l is the harmonic number. This expression gives high m-numbers (about $10l$ for TFTR).

Table I. Numerically Computed Maximum Growth Rates, Normalized to the Deuterium Cyclotron Frequency, for the Fusion Products: Tritium, ^{3}He and Protons
(The growth rates are computed for perpendicular propagation, $\theta = 90°$. The maximum growth rate is reached at the frequency $\omega = l\omega_{c\{T,^3He,p\}} - \omega_D \simeq kv_A$.)

Species	$l = 1$	$l = 2$	$l = 3$
Tritium	1.3×10^{-3}	2.0×10^{-3}	8.8×10^{-4}
^{3}He	2.6×10^{-3}	2.5×10^{-3}	2.1×10^{-3}
Protons	2.2×10^{-2}	3.6×10^{-2}	4.6×10^{-2}

In the experiments in TFTR, for example, in the shots 73255, 73265, 73273 [7] and 73266 [8], the initial spectrum is dominated by low harmonics of the alpha particle and/or ^{3}He cyclotron frequencies, evaluated at the outer midplane edge. Our numerical results show that the fast magnetoacoustic waves are destabilized for those frequencies, cf. Table I for tritons, ^{3}He nuclei and protons and Fig. 1 for alpha particles. Note that the instability driven by super-Alfvénic protons gives rise to relatively high growth rates.

In Ref. [13] the instability growth rate has been calculated in the straight magnetic field approximation and the instability growth rates obtained do not fulfil the rapid instability condition, $\gamma > \tau_b^{-1}$, which implies the condition $\gamma/\omega_{c\alpha} > 4 \times 10^{-4}$ for the normalized growth rate (for the TFTR parameters used in the calculations of Ref. [13]: $q \simeq 3.75$, $v_d = 0.5 \times 10^7$ m/s, $\omega_{c\alpha} = 2.4 \times 10^8$ Hz and $R = 2.5$ m). The maximum growth rate for the alpha particle driven instability of Ref. [13] is about an order of magnitude too low.

Our numerical results show that the inclusion of the toroidal effects in the resonance condition gives considerably larger growth rates, about 1 or 2 orders of magnitude higher than the fast ion bounce frequency. Figure 2 shows the instability growth rates calculated for the harmonic number $l = 4$ and for different angles of propagation: $\theta = 95$, 92, 90, 88 and 85° (from right to left). The growth rate is maximal for $\theta \simeq 90°$ (perpendicular propagation), which is in agreement with the results of Ref. [12] for the JET DT parameters.

The doublet structure of the ICE signal in JET has been attributed to the destabilization of waves with $\omega = l\omega_{c\alpha} \pm |\omega_D|$, where the $\pm$ in front of the drift frequency ω_D corresponds to different signs of the poloidal number m [12]. In the case of the fusion product induced ICE in TFTR, the doublet structure is not observable because the doublet width $\delta_D = 2\omega_D$ is much smaller than the wave frequency. Taking $\chi = v_\parallel/v \simeq v_d/v_\alpha = 0.4$ and $\omega \simeq kv_A \simeq l\omega_{c\alpha}$, we obtain $\delta_D/\omega \simeq 1.5 \times 10^{-2}$, which seems to be difficult to discern in the experimental observations.

Let us now analyse the scaling of the ICE power with the neutron emission rate (a measure of fusion reactivity and fast ion density). The experimentally observed ICE signal in JET is proportional to the neutron rate over six orders of magnitude. In contrast to JET, the correlation between the ICE signals and neutron rates in TFTR appears to be sublinear

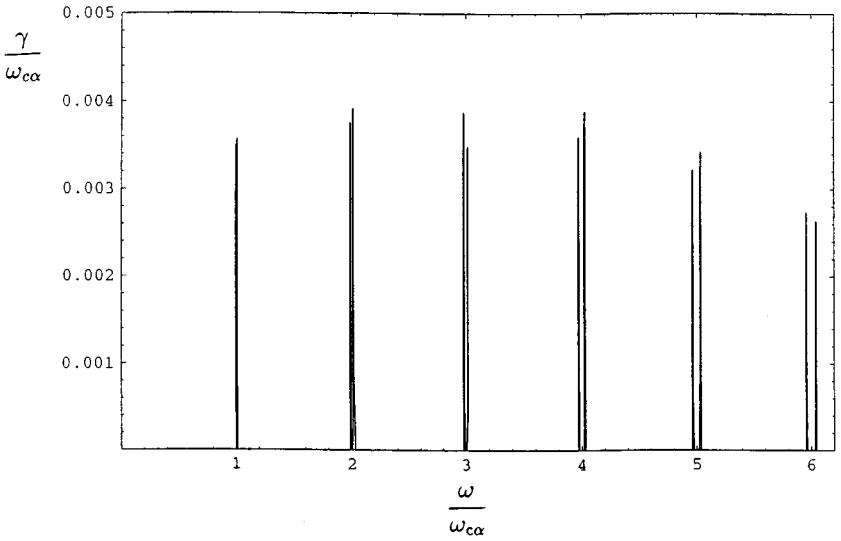

FIG. 1. Instability growth rate $\gamma/\omega_{c\alpha}$ for alpha particle driven MCI in TFTR as a function of ω. The two peaks below and above each harmonic correspond to positive and negative poloidal wavenumbers.

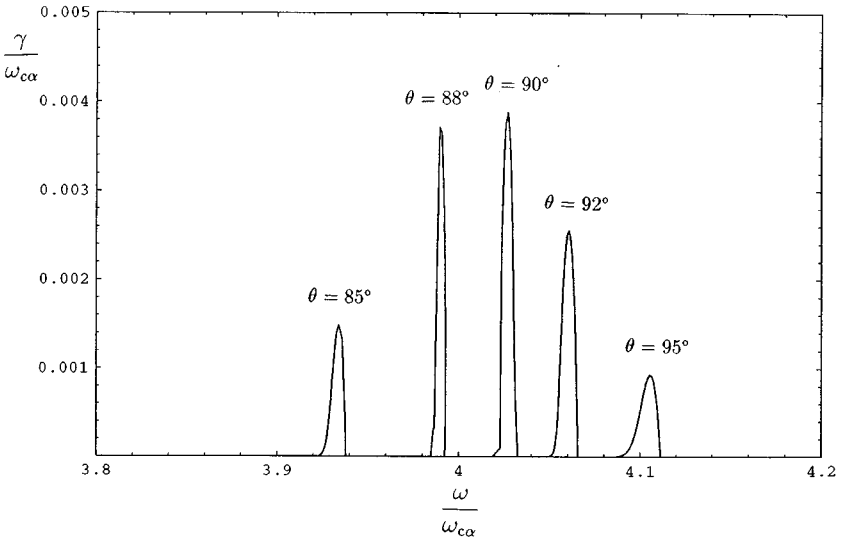

FIG. 2. Growth rate as a function of the frequency for the angles of propagation $\theta = 95$, 92, 90, 88 and 85° (from right to left), harmonic number $l = 4$ and positive values of the poloidal number m. Note that the growth rate is maximum for perpendicular propagation, i.e. $\omega - l\omega_{c\alpha} = \omega_D$.

and scattered. Assuming that the emission power is proportional to the growth rate, the experimentally observed scaling of the ICE intensity with the neutron rate can be qualitatively explained by examining the linear instability growth rate scaling with the fast ion density.

The perturbative model, (14), predicts that for small alpha particle densities the growth rate varies linearly with n_α. However, as we increase the alpha particle to background ion density ratio n_α/n_i, the growth rate variation with n_α becomes sublinear. For sufficiently high fast ion density the growth rate is independent of n_α/n_i. Figure 3 shows the maximum linear instability growth rate γ_{max} as a function of the alpha particle to background ion density ratio n_α/n_i for the TFTR DT parameters listed above,

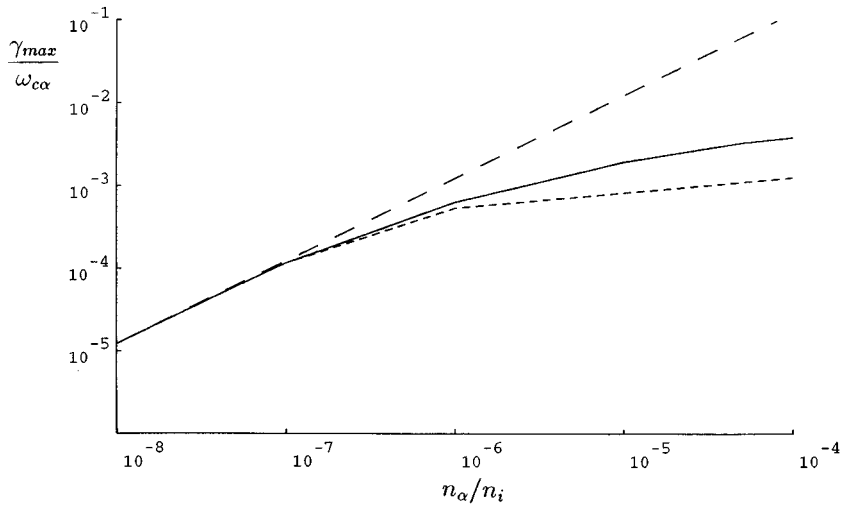

FIG. 3. Maximum instability growth rate $\gamma_{\max}/\omega_{c\alpha}$ as a function of the alpha particle concentration n_α/n_i calculated for the harmonic number $l = 4$. The long dashed and short dashed curves correspond to $\gamma_{\max} \propto n_\alpha/n_i$ and the perturbatively calculated growth rate, γ^α, respectively. The solid curve shows the result of a numerical calculation.

perpendicular propagation and harmonic number $l = 4$, compared with $\gamma_{\max} \propto n_\alpha/n_i$ (long dashed curve) and the perturbatively calculated growth rate γ^α (short dashed curve). The numerically calculated growth rate (solid curve) shows a sublinear dependence on the fast ion density.

The experimentally observed fusion product driven ('early') ICE does not persist very long in TFTR after the onset of beam heating [7]. In Ref. [13] it is shown, in the straight magnetic field approximation, that if the alpha particles are sub-Alfvénic, the instability is very sensitive to the collision induced spreading of the alpha particle velocity distribution. Immediately after the onset of neutral beam heating only the fusion products that follow barely trapped orbits reach the plasma edge. Thus, the energetic ion population at the edge is initially very narrow and can therefore excite the MCI. The distribution function widens gradually owing to collisions, until the instability can no longer be excited.

In our calculation, the width of the distribution is determined by the parallel velocity spread. Our numerical results confirm the conclusions of Ref. [13] that the instability growth rate is reduced when the fast ion parallel velocity spread is increased. However, this reduction is not as strong as Ref. [13] suggested. Figure 4 shows the instability growth rate γ normalized to the alpha particle cyclotron frequency $\omega_{c\alpha}$, as a function of frequency for different values of the parallel velocity spread v_s. The growth rate is shown for $v_s/u = 0.05$ (solid curve), $v_s/u = 0.1$ (dashed curve) and $v_s/u = 0.15$ (dotted curve). The degradation of the growth rate as we increase the parallel velocity spread is clear, but it is not as dramatic as in the straight magnetic field approximation [13]. The dependence of the growth rate on the velocity spread v_s can been investigated also for super-Alfvénic ions, by reducing the Alfvén velocity, and keeping the other parameters the same so that the alpha particle velocity becomes slightly higher than v_A. Even in this case we observe a slight degradation of the growth rate with increasing v_s, but the growth rates remain high, see Fig. 5.

Comparing the results of the related papers of Gorelenkov and Cheng [14, 15], and our work, we note the large difference in the resulting growth rates. In Ref. [14] the bounce averaged approach is used, implying that the growth rate of the instability is small as compared with the bounce frequency. Thus, the bounce averaged approach is applicable for large interaction times. In contrast, the local approach used in the present work is applicable for short interaction times, and thus for growth rates larger than the bounce frequency. An application of the local approach is motivated by the fact that, as was shown in Refs [14–17], the mode considered is localized at the outer edge of the plasma, and therefore the interaction time is short. Mathematically, the large difference between the growth rates calculated in this article and those of Gorelenkov and Cheng is partly

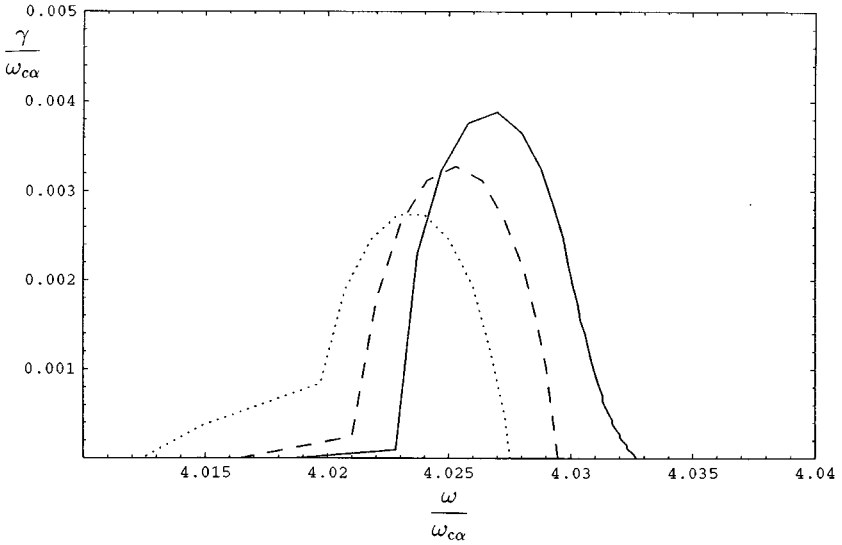

FIG. 4. Instability growth rate $\gamma/\omega_{c\alpha}$ for different values of the parallel velocity spread v_s. The growth rate is shown for various values of v_s/u: 0.05, solid curve; 0.1, dashed curve; 0.15, dotted curve.

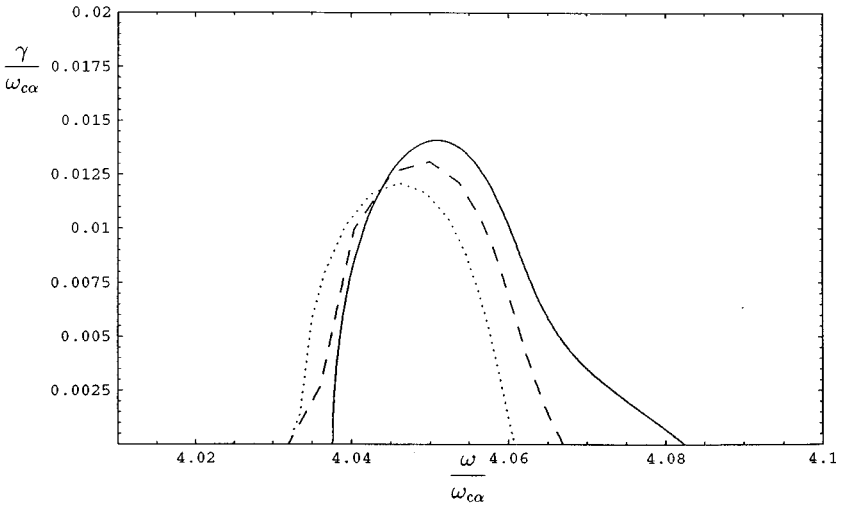

FIG. 5. Instability growth rate $\gamma/\omega_{c\alpha}$ for different values of the parallel velocity spread v_s calculated for super-Alfvénic particles by using the Alfvén velocity $v_A = 1.1 \times 10^6$ m/s. The growth rate is shown for various values of v_s/u: 0.05, solid curve; 0.1, dashed curve; 0.15, dotted curve.

due to a rapidly oscillating exponential function in Eq. (40) of Ref. [14], the integral of which is small and makes the growth rates small.

Quantitatively, comparing the expressions for the growth rate, Eq. (50) of Ref. [15] and our Eq. (14), we find that the main difference is due to the factor

$$I^2 = 8\pi/[|\mathrm{d}(l\omega_c + \omega_D)/\mathrm{d}t|^3 + C|\mathrm{d}^2(l\omega_c + \omega_D)/\mathrm{d}t^2|^2]^{1/3}$$

with $C = 2.6943$. Another difference is that, in Ref. [14], the mode structure is included in the bounce averaged expression of the growth rate, which has a slightly stabilizing effect. In our case, only the local value of the mode field is taken into account.

The ratio of the bounce averaged to the local growth rate is

$$\frac{\gamma_b}{\gamma_\ell} \simeq \frac{1}{8\pi^3}\frac{v_d}{qR_0} I^2 \left|\frac{\mathrm{d}\Omega}{\mathrm{d}\chi}\right|_{\chi_r} \qquad (Cont.)$$

Table II. Numerically Computed Maximum Growth Rates, Normalized to the Deuterium Cyclotron Frequency, for the Injected Beam Ions: Deuterium and Tritium
(The growth rates are computed for perpendicular propagation, $\theta = 90°$. The maximum growth rate is reached at the frequency $\omega = l\omega_{\rm cb} - \omega_{\rm D}$.)

Species	$l=1$	$l=2$	$l=3$	$l=4$	$l=5$	$l=6$
Deuterium	6×10^{-4}	1.5×10^{-3}	3.8×10^{-3}	7.5×10^{-3}	1.4×10^{-2}	1.5×10^{-2}
Tritium	2×10^{-3}	2.4×10^{-3}	1.2×10^{-3}	5.5×10^{-3}	6.3×10^{-3}	4.8×10^{-3}

$$\times \sqrt{\frac{2}{\pi}} \int \frac{r\,{\rm d}r}{r_\star \Delta} \exp\left[-2(r-r_\star)^2/\Delta^2\right](1-r^2/a^2)^{3.75} \tag{17}$$

where $\Omega = \omega - k_\parallel v_\parallel - s\omega_{{\rm c}\alpha} - \omega_{\rm D}$ and $\Delta^2/a^2 = [2\sigma_{\rm i}/(1+\sigma_{\rm i})]^{1/2}/[m(1+\sigma_{\rm i})]$ with $\sigma_{\rm i} = 0.2$ [14]. When $k_\parallel = 0$, we can estimate that $|{\rm d}\Omega/{\rm d}\chi|_{\chi=\chi_{\rm r}} \simeq |2\omega_{\rm D}\chi_{\rm r}/(\chi_{\rm r}^2+1)|$. Estimating the expression for I^2 at the outer midplane edge, $\theta \simeq 0$, we obtain

$$I^2 \simeq 8\pi \Big/ \left[C^{1/3}\omega_{\rm D0}^{2/3}({\rm d}\theta/{\rm d}t)^{4/3}\right]$$

$$\simeq 8\pi(qR/v_{\rm d})^{4/3} \Big/ \left(C^{1/3}\omega_{\rm D0}^{2/3}\right)$$

where $\omega_{\rm D0}$ denotes the toroidal drift frequency taken at $\theta = 0$ and we have assumed that $v_\parallel \simeq v_{\rm d}$. Taking the parameters for the alpha particle driven instability, we find the ratio of the growth rates to be of the order of $\gamma_{\rm b}/\gamma_\ell \simeq 5\times10^{-3}$. Thus, the inclusion of toroidal drift and the application of the local approach yield a growth rate that is more than two orders of magnitude larger than the one calculated with the bounce averaged approach. This result is obtained by comparing the expressions for the perturbatively calculated growth rates in the two cases. The numerical results presented here and in Ref. [14] differ even more, mainly because the alpha particle distribution functions used in the two articles are different and also because the growth rates shown in Fig. 1 are obtained from a numerical solution of the dispersion equation and not from a perturbative solution.

3.2. Beam ion driven ICE

We turn now to the part of the ICE spectrum that has been observed at TFTR in connection with NBI heating when a high power beam consisting of deuterium or tritium atoms is injected parallel to the magnetic axis. The beam atoms propagate at an angle of 45° to the magnetic field in the edge plasma [9].

A mechanism for the beam driven excitation of ICE in TFTR has been proposed by Dendy et al. [9] in the straight magnetic field approximation. It

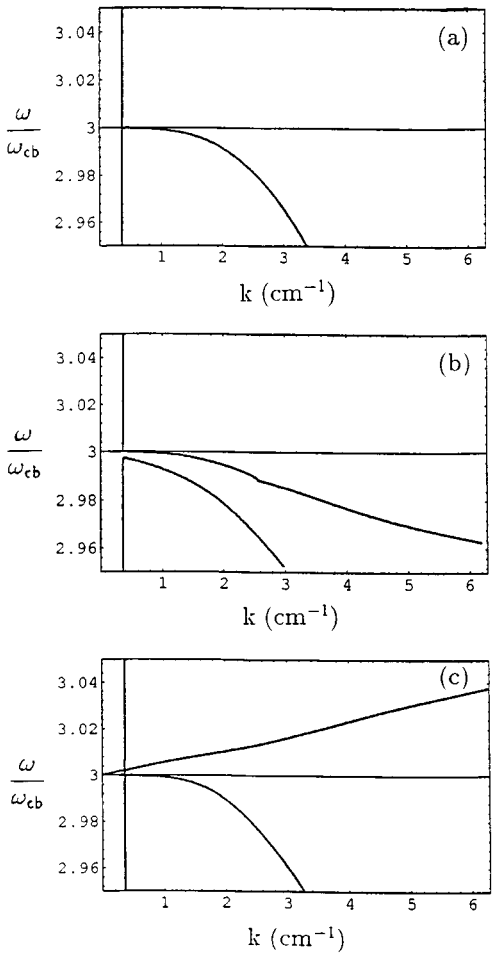

FIG. 6. Dependence of the real part of the frequency on the wavenumber k for a background ion beta of 10^{-3} near the harmonic line $l = 3$: (a) without beam ions, (b) with a beam ion population having a relative density $n_{\rm b}/n_{\rm i} = 10^{-2}$ and for positive poloidal numbers m, (c) with the same beam ion population but for negative poloidal numbers m. The beam and bulk ions are deuterium, and the wave propagation is perpendicular to the magnetic field.

has been concluded that the instability responsible for the emission excites a beam supported, predominantly electrostatic wave. This instability requires a narrow velocity space distribution of the beam ions and it is modelled by a drifting ring distribution function in the numerical calculations. However, for the lowest harmonics, the numerically calculated instability growth rates in Ref. [9] are rather low and barely satisfy the condition for rapid instability implying that, for the parameters used in Ref. [9], $\gamma/\omega_{\rm cb} > 1.7 \times 10^{-4}$.

Our calculations generalize the approach of Ref. [9] to the toroidal case, by including the toroidal effects into the resonance condition. The parameters used in the calculations are, following Ref. [9], magnetic field $B = 5$ T, Alfvén velocity $v_{\rm A} = 2 \times 10^7$ m/s, background ion beta $\beta_{\rm i} = 10^{-3}$, ratio of ion to electron temperature $T_{\rm i}/T_{\rm e} = 2$, beam ion injection energy $T_{\rm D} = T_{\rm T} = 120$ keV (where the subscripts 'D' and 'T' denote deuterium and tritium beam ions, respectively). The fast ion densities are assumed to be $n_{\rm D} = n_{\rm T} = 10^{-2} n_{\rm i}$. The beam ion velocity spread and drift are $v_{\rm s}/u = 10^{-2}$ and $v_{\rm d}/u = 1$, respectively.

We have calculated the instability growth rate γ by solving Eq. (1) for a drifting ring distribution function of the beam ions. The inclusion of the toroidal drift frequency increases the instability growth rate (compared with the calculations using the straight magnetic field approximation) giving larger growth rates than the bounce frequency, Table II.

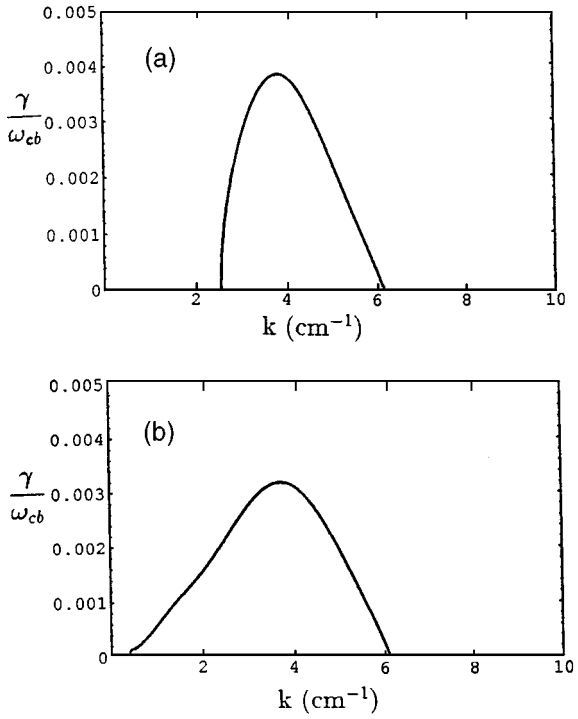

FIG. 7. Beam driven instability growth rate for (a) positive and (b) negative poloidal wavenumbers. The plasma parameters are identical to those in Fig. 6.

Figures 6 and 7 show the real and imaginary parts of the frequency, as functions of the wavenumber near the harmonic line $l = 3$. The numerical solution of Eq. (1) in the absence of beam ions is shown in Fig. 6(a). The presence of the energetic beam ion contribution in Eq. (1) introduces new wave branches that can be unstable. When the beam ion distribution is given by Eq. (9) the location of these new (unstable) wave branches is as shown in Figs 6(b) and (c), where the real part of the wave frequency is plotted near the harmonic line $l = 3$ as a function of the wavenumber for positive and negative poloidal numbers m. The corresponding instability growth rates are shown in Fig. 7. Also here, the maximum growth rates occur for nearly perpendicular propagation: $\omega = l\omega_{\rm cb} \pm |\omega_{\rm D}|$, but the peaks are much broader than in the fusion driven case. The phase velocity of the destabilized waves is close to the beam ion speed, $\omega/k \simeq v_{\rm b}$ and, since the beam ions are sub-Alfvénic, the phase velocities of these waves are about an order of magnitude smaller than in the fusion driven case (where $\omega/k \simeq v_{\rm A}$).

Figure 8 shows the numerically (solid curve) and perturbatively (dashed curve) calculated growth rates $\gamma^{\rm b}$ for deuterium injection as functions of the fast ion density, calculated for the harmonic number $l = 4$ and positive poloidal wavenumbers m. For the TFTR parameters, the scaling of the growth rate with the fast ion density is sublinear, and the growth rate is larger than the bounce frequency even for very low beam ion density, for example, $n_{\rm D} = n_{\rm T} \gtrsim 10^{-4} n_{\rm i}$.

4. CONCLUSIONS

The main result of this article is that inclusion of the toroidal effects (curvature and ∇B drift) into the resonance condition greatly increases the instability growth rate of the fast magnetoacoustic waves. The growth rates are calculated by numerically solving the dispersion equation for magnetoacoustic waves, using the parameters of the TFTR DT experiment. A perturbative analysis of the dispersion relation of perpendicularly propagating waves yields growth rates with the same qualitative behaviour as the numerically computed ones.

The scaling of the growth rate with the fast ion density depends mainly on the local (edge) Alfvén

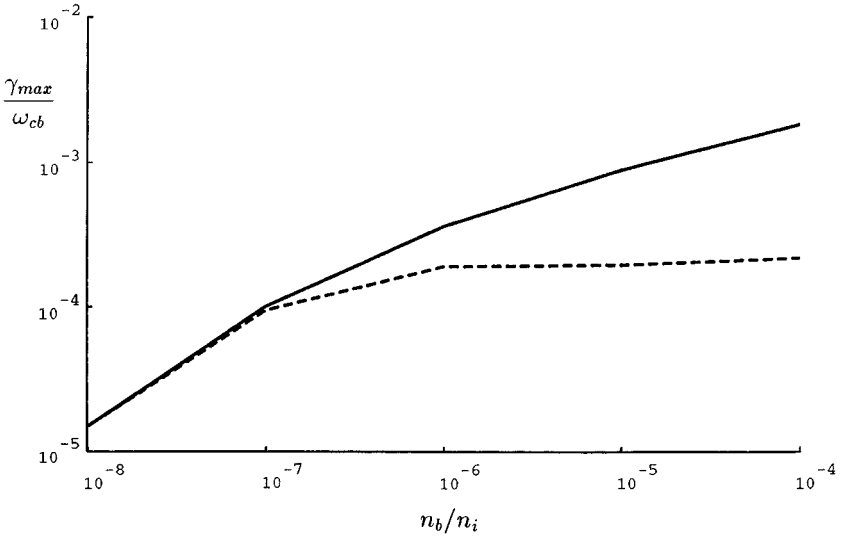

FIG. 8. Deuterium beam driven instability growth rate $\gamma_{\max}/\omega_{\rm cb}$, calculated numerically (solid curve) and perturbatively (dashed curve), as a function of the beam ion concentration $n_{\rm b}/n_{\rm i}$, calculated for the harmonic number $l = 4$ and positive poloidal wavenumber m.

velocity. For very low fast ion density n_α, the dependence is linear, but becomes sublinear as n_α is increased. If the Alfvén velocity is low compared with the fast ion velocity, the linear correlation is sustained even for moderate values of the fast ion densities, which explains the difference between the scalings of the growth rate with the fast ion density in JET and TFTR.

The growth rate is decreasing with increasing velocity spread at a rate that depends on the ratio of alpha particle to Alfvén velocity $v_\alpha/v_{\rm A}$. This result is qualitatively consistent with the conclusions of Ref. [13], that the MCI is suppressed if the parallel velocity spread of the sub-Alfvénic fusion product is increased. However, the growth rate reduction is not as dramatic in the toroidal case as it was in the cylindrical limit, and cannot alone account for the suppression of the MCI. For a better understanding of this feature, a realistic distribution model for the fast ions is necessary.

The doublet structure of the ion cyclotron emission lines is not observable because the drift velocities of the sub-Alfvénic beam ions and fusion products, driving the ICE in TFTR, are too small compared with the wave frequency.

The ICE can also be driven by injected sub-Alfvénic beam ions, in the outer midplane edge in TFTR. An excitation mechanism outlined in Ref. [9], and generalized in this article to the toroidal case, provides an explanation of the observed beam driven ICE. Compared with the cylindrical case considered in Ref. [9], the growth rate is greatly increased and reaches its maximum for nearly perpendicular propagation.

Appendix

THE DIELECTRIC TENSOR OF A FAST PARTICLE POPULATION WITH A DRIFTING RING DISTRIBUTION FUNCTION

We use the drifting ring model, Eq. (9), for the energetic ion distribution function, viz.

$$f_\alpha = \frac{1}{2\pi^{3/2} u v_{\rm s}} \exp\left(-\frac{(v_\parallel - v_{\rm d})^2}{v_s^2}\right)\delta(v_\perp - u). \qquad (18)$$

The dielectric tensor components are, [12],

$$\epsilon_{ij}^\alpha = \sum_{s=-\infty}^{\infty} \frac{\omega_{{\rm p}\alpha}^2}{\omega^2} \int {\rm d}^3 v \frac{v_\perp^2\, M_{ij}(s,\xi)}{\omega - s\omega_{{\rm c}\alpha} - k_\parallel v_\parallel - \omega_{\rm D}} \times \left(\omega \frac{\partial f_\alpha}{\partial E} + \frac{\omega - k_\parallel v_\parallel - \omega_{\rm D}}{B_0} \frac{\partial f_\alpha}{\partial \mu}\right) \qquad (19)$$

where

$$M_{ij}(s,\xi) = \begin{pmatrix} (s^2/\xi^2) J_s^2(\xi) & -({\rm i}s/\xi) J_s(\xi) J_s'(\xi) \\ ({\rm i}s/\xi) J_s(\xi) J_s'(\xi) & [J_s'(\xi)]^2 \end{pmatrix} \qquad (20)$$

and $\xi = k_\perp v_\perp/\omega_{c\alpha}$, $\omega_D = -mv_D/r$, $v_D = v^2(1+\chi^2)/(2\omega_{c\alpha}R)$ is the toroidal drift velocity, $J_s(\xi)$ is the Bessel function of the first kind and of order s, and R is the major radius of the torus. Changing variables to $v_\perp$ and $v_\parallel$ gives

$$\epsilon_{ij}^\alpha = 2\pi \sum_{s=-\infty}^{\infty} \frac{\omega_{p\alpha}^2}{\omega^2} \int \mathrm{d}v_\parallel \, \mathrm{d}v_\perp \, \frac{v_\perp^2 (A+B)}{\Omega} M_{ij}(s,\xi) \tag{21}$$

where

$$A = (\omega - k_\parallel v_\parallel - \omega_D)\frac{\partial f_\alpha}{\partial v_\perp}$$

$$B = (k_\parallel v_\parallel + \omega_D)\frac{v_\perp}{v_\parallel}\frac{\partial f_\alpha}{\partial v_\parallel}$$

and

$$\Omega = \omega - s\omega_{c\alpha} - k_\parallel v_\parallel - \omega_D.$$

Introducing the notation $t = (v_\parallel - v_d)/v_s$, Ω can be rewritten as

$$\begin{aligned}\Omega &= \frac{k_\perp}{R\omega_{c\alpha}}(v_\parallel - v_{\parallel 1})(v_\parallel - v_{\parallel 2}) \\ &= \frac{k_\perp v_s^2}{R\omega_{c\alpha}}(t-t_1)(t-t_2)\end{aligned} \tag{22}$$

with

$$t_{1,2} = \frac{R\omega_{c\alpha}}{2k_\perp v_s}\left(k_\parallel \pm \sqrt{k_\parallel^2 - 4\frac{k_\perp \Delta\omega}{R\omega_{c\alpha}}}\right) - \frac{v_d}{v_s} \tag{23}$$

and

$$\Delta\omega = \omega - l\omega_{c\alpha} + \frac{k_\perp u^2}{2R\omega_{c\alpha}}. \tag{24}$$

The integrals can now be written in terms of plasma dispersion functions. Using the notation $Z_j = Z(t_j)$, where Z is the plasma dispersion function, and $z_\alpha = k_\perp u/\omega_{c\alpha}$, we obtain

$$\epsilon_{11}^\alpha = -\frac{s^2}{z_\alpha}\frac{\omega_{p\alpha}^2}{\omega^2}\left(\frac{J_s^2}{z_\alpha}\mathcal{P} + \frac{\mathrm{d}J_s^2}{\mathrm{d}z_\alpha}\mathcal{Q} + J_s^2\mathcal{T}\right) \tag{25}$$

$$\begin{aligned}\epsilon_{22}^\alpha = &-\frac{\omega_{p\alpha}^2}{\omega^2} \\ &\times \left((J_s')^2\mathcal{P} + \frac{\mathcal{Q}}{z_\alpha}\frac{\mathrm{d}}{\mathrm{d}z_\alpha}[z_\alpha^2 (J_s')^2] + (J_s')^2 z_\alpha \mathcal{T}\right)\end{aligned} \tag{26}$$

$$\begin{aligned}\epsilon_{21}^\alpha = &-\mathrm{i}s\frac{\omega_{p\alpha}^2}{\omega^2} \\ &\times \left(\frac{J_s J_s'}{z_\alpha}\mathcal{P} + \frac{\mathcal{Q}}{z_\alpha}\frac{\mathrm{d}}{\mathrm{d}z_\alpha}(z_\alpha J_s J_s') + J_s J_s' \mathcal{T}\right)\end{aligned} \tag{27}$$

where the functions $\mathcal{P}$, $\mathcal{Q}$ and $\mathcal{T}$ are defined as

$$\begin{aligned}\mathcal{P} = \frac{2u^2}{v_s^2}\Bigg(&k_\parallel v_s S F(t_1 Z_1 - t_2 Z_2) \\ &- (1 + A_0 Z_1 + B_0 Z_2) - \frac{u^2}{2v_s^2} \\ &\times (A_1 Z_1 + B_1 Z_2 + C_1 Z_3)\Bigg)\end{aligned} \tag{28}$$

$$\mathcal{Q} = 1 + s\omega_{c\alpha} S F(Z_1 - Z_2) \tag{29}$$

$$\begin{aligned}\mathcal{T} = &2s\omega_{c\alpha}\frac{u}{R}S^2F^2 \\ &\times [2 + t_1 Z_1 + t_2 Z_2 + F(Z_1 - Z_2)]\end{aligned} \tag{30}$$

and the coefficients are

$$A_0 = t_1 + t_2 - t_3 - B_0 \tag{31a}$$

$$B_0 = t_2(t_1 - t_3)F \tag{31b}$$

$$A_1 = C_1\frac{t_1(t_2 - t_3)}{t_3}F \tag{31c}$$

$$B_1 = C_1\frac{t_2(t_3 - t_1)}{t_3}F \tag{31d}$$

$$C_1 = \frac{t_3(t_1 - t_2)}{t_1^2(t_2 - t_3) + t_2^2(t_3 - t_1) + t_3^2(t_1 - t_2)} \tag{31e}$$

with $S = R\omega_{c\alpha}/k_\perp v_s^2$, $F = 1/(t_1 - t_2)$ and $t_3 = -v_d/v_s$.

The expressions for the dielectric tensor elements, Eqs (25) to (27), reduce to those of the cylindrical case (given in Ref. [11], Eqs (11) to (13)), in the limit $R \to \infty$.

In the expression for the plasma dispersion function (used in ϵ_{ij}^α)

$$Z_i(\omega) = Z(t_i(\omega)) = \frac{1}{\sqrt{\pi}}\int_{-\infty}^{\infty}\frac{\mathrm{e}^{-x^2}\mathrm{d}x}{x - t_i(\omega)} \tag{32}$$

it is implicitly assumed that $\mathrm{Im}\, t_i > 0$. For $\mathrm{Im}\, t_i < 0$ the function $Z(t_i)$ must be replaced with $Z(t_i^\star)^\star$, where the asterisk denotes complex conjugation [18]. The expression for $Z_i(\omega)$ is derived for $\mathrm{Im}\,\omega > 0$ and must be analytically continued for $\mathrm{Im}\,\omega < 0$. Since the function $t_i(\omega)$ contains a square root, the branch cut must be chosen so that $Z(t_i(\omega))$ is continuous. The standard choice for the branch cut (for real and negative arguments) makes Z_i discontinuous when moving from the upper to the lower half-plane. Thus, in the expression for t_i we should use the branch cut

$${}^{\mathrm{new}}\sqrt{x} = \begin{cases} \sqrt{\mathrm{i}}\sqrt{\dfrac{x}{\mathrm{i}}} & \text{if} \quad k_\perp < 0 \\ \sqrt{\dfrac{1}{\mathrm{i}}}\sqrt{\mathrm{i}x} & \text{if} \quad k_\perp \geq 0. \end{cases}$$

ACKNOWLEDGEMENTS

This work has been supported by the European Union under an association contract between Euratom and Sweden.

REFERENCES

[1] TFTR TEAM (presented by G.J. GREENE), in Controlled Fusion and Plasma Heating (Proc. 17th Eur. Conf. Amsterdam, 1990), Vol. 14B, Part IV, European Physical Society, Geneva (1990) 1540.
[2] CAUFFMAN, S.R, Ion Cyclotron Emission from Fusion Plasmas, PhD Thesis, Princeton Univ., NJ (1997).
[3] COTTRELL, G.A., DENDY, R.O., Phys. Rev. Lett. **60** (1988) 33.
[4] COTTRELL, G.A., et al., Nucl. Fusion **33** (1993) 1365.
[5] SEKI, M., et al., Phys. Rev. Lett. **62** (1989) 1989.
[6] DUONG, H.H., et al., Nucl. Fusion **33** (1993) 749.
[7] CAUFFMAN, S., MAJESKI, R., Rev. Sci. Instrum. **66** (1995) 817.
[8] CAUFFMAN, S., et al., Nucl. Fusion **35** (1995) 1597.
[9] DENDY, R.O., et al., Phys. Plasmas **1** (1994) 3407.
[10] BUDNY, R.V., et al., Nucl. Fusion **32** (1992) 429.
[11] DENDY, R.O., et al., Phys. Plasmas **1** (1994) 1918.
[12] FÜLÖP, T., et al., Nucl. Fusion **37** (1997) 1281.
[13] McCLEMENTS, K.G., et al., Phys. Plasmas **3** (1996) 543.
[14] GORELENKOV, N.N., CHENG, C.Z., Phys. Plasmas **6** (1995) 1961.
[15] GORELENKOV, N.N., CHENG, C.Z., Nucl. Fusion **35** (1995) 1743.
[16] COPPI, B., Phys. Lett. A **172** (1993) 439.
[17] COPPI, B., et al., Phys. Fluids **29** (1986) 4060.
[18] STIX, T.H., Waves in Plasmas, American Institute of Physics, New York (1992).

(Manuscript received 16 June 1997
Final manuscript accepted 27 January 1998)

E-mail address of T. Fülöp:
tunde@elmagn.chalmers.se

Subject classification: D3, Tt